# Distributed Acoustic Sensing (DAS) for Longwall Coal Mines

Derrick Chambers[1*], Alexander Ankamah[2], Ahmad Tourei[3], Eileen R. Martin[3], Tim Dean[4], Jeffrey Shragge[3], John A Hole[3], Rafal Czarny[5], Gareth Goldswain[5], Jako du Toit[5], M. Shawn Boltz[1], James McGuiness[4]

1- National Institute for Occupational Safety and Health, 315 E Montgomery Av, Spokane, WA, 99207, USA

2- Virginia Tech, 290 College Ave, Blacksburg, VA, 2406, USA

3- Colorado School of Mines, 1500 Illinois St, Golden, CO, 80401, USA

4- Anglo American, 11/201 Charlotte St, Brisbane City, QLD, 4000, Australia

5- Institute of Mine Seismology, 10 Church Street, Kingston, Tasmania, 7050, Australia

*- Corresponding author (derchambers@cdc.gov)

Seismic monitoring of underground longwall mines can provide valuable information for managing coal burst risks and understanding the ground response to extraction. However, the underground longwall mine environment poses major challenges for traditional in-mine microseismic sensors including the restricted use of electronics due to potentially explosive atmospheres, the need to frequently and quickly relocate sensors as rapid mining progresses, and source parameter errors associated with complex time-dependent velocity structure. Distributed acoustic sensing (DAS), a technology that uses rapid laser pulses to measure strain along fiber-optic cables, shows potential to alleviate these shortcomings and improve seismic monitoring in coal mines when used in conjunction with traditional monitoring systems. Moreover, because DAS can acquire measurements that are not possible to record with traditional seismic sensors, it also enables entirely new monitoring approaches. This work demonstrates several DAS deployment strategies such as deploying fiber on the mine floor, in boreholes drilled from the surface and from mine level, on the longwall mining equipment, and wrapped around secondary support cans. Although there are several data processing and deployment improvements needed before DAS-based monitoring can become routine in underground longwall mines, the findings presented here can aid decision makers in assessing the potential of DAS to meet their needs and help guide future deployment designs.

**Keywords:** longwall mining; underground coal mining; distributed acoustic sensing; distributed fiber-optic sensing

# 1 Introduction

Many underground mines experience a variety of dynamic failures that cause violent, near-instantaneous damage to mine openings. In hardrock mines, these failures are termed “rockbursts,” and though certainly not a solved problem, significant progress has been made in managing and reducing rockburst risks in the past several decades [1,2]. A key component of this success has come from improvements in, and increased adoption of, seismic monitoring. Monitoring seismicity can provide an increased understanding of the earth's reaction to resource extraction, can be used to forecast seismic hazards to guide mining and ground control decisions, inform mine re-entry protocols, as well as a variety of other useful functions [3–5].

Several studies have demonstrated similar uses of microseismic monitoring in coal mines, which can also experience violent dynamic failures known as “coal bursts.” Various uses of microseismic monitoring in coal mines include: detecting fracturing associated with failure of thick strata in the overburden [6] and water inflows [7]; imaging high stress areas [8]; forecasting bump risk [9]; identifying the activation of seismogenic geological features [10]; and other ground control objectives. Despite an abundance of promising studies, the coal mining industry has been slow to adopt seismic monitoring. Swanson et al. [11] highlight some of the challenges that impede longwall mines from routinely operating the same types of in-mine networks used in hardrock mining, which include: the tendency of coal mines to be much larger and mine more rapidly than typical hardrock mines; regulations restricting the use of electronics in coal mines due to potentially explosive atmospheres; and difficulty locating events in the complex, time-varying media associated with coal extraction in faulted sedimentary environments. Surface-based deployments [12–14] overcome some of these shortcomings, but they typically are not as sensitive, do not achieve the same event location accuracy, and are more affected by complex near-surface geologies.

Distributed acoustic sensing (DAS), a subset of distributed fiber-optic sensing (DFOS) [15], uses rapid laser pulses to monitor strain and vibration in fiber-optic cable. DAS could play a role in making seismic monitoring in underground coal mines more feasible for the following reasons. First, DAS-compatible cable is already widely used for data transfer in underground coal mines. Unlike the electronics associated with traditional seismic systems, these cables pose no risk to initiating an explosion and can be placed anywhere in a coal mine, provided that the device acquiring the recordings, known as a DAS interrogator unit (IU), is located in the intake air. Second, because DAS systems can monitor tens of kilometers of cable (hundreds

with some newer systems), monitoring large areas and rapid mining rates becomes much less of an issue than with traditional sensors. Moreover, spatially dense DAS recordings are better able to observe and quantify propagation complexity than sparse point sensors.

Published studies have used DAS for monitoring induced seismicity related to hydrocarbon extraction [16], recording regional and global earthquakes [17], determining seismic site characteristics for earthquake hazard assessment [18], and several other geophysical applications [19]. A few recent works have documented DAS deployments in underground mines, such as in the Sanford Underground Research Facility [20], an active room-and-pillar limestone and dolomite mine [21], and an underground hardrock mine [22]. Examples of DAS deployments in or above coal mines are even more limited. Luo and Duan [23] used DAS on a cable installed in a borehole and trenched above a mine to monitor caving associated with longwall coal mining. Chambers and Shragge [24] deployed a DAS-based seismoacoustic array, discussed in **Section 6**, to monitor coal bursts occurring on the mining face.

Each of the aforementioned studies demonstrates the potential of DAS for mining applications. However, before DAS can become a routine monitoring tool in longwall coal mines, further work is needed to develop viable deployment strategies as well as data processing and management approaches. This work presents field trials of several types of DAS deployments in active longwall coal mines and is organized as follows. First, longwall mining and the relevant concepts to this study, as well as DAS fundamentals for microseismic monitoring, are reviewed. The following sections describe seven DAS deployments which included deploying cable on the mine floor, in a vertical and directional borehole drilled from the surface, in a near-horizontal borehole drilled from mine level, a seismoacoustic array deployed on the longwall face, fiber deployed in the longwall cable tray, and fiber wrapped around support cans. A discussion of the strengths and shortcomings of each deployment, as well as the monitoring objectives they could meet, is then offered. Finally, key challenges and research directions that could help accelerate adoption of DFOS technology in coal mines are highlighted.

## 2 Background

### *2.1 Longwall mining*

Longwall mining is an efficient, high-extraction mining method for exploiting thin-seam deposits such as coal, pot ash, and soda ash. Although more capital intensive, the longwall method has yielded significant safety and operational improvements over conventional approaches such as room-and-pillar mining [25]. The main components of a longwall are a line of shields, a cutting device, and an armored conveyor belt (Fig. 1 a and b). The shields support the roof and provide a protected travel way. They also incrementally advance as extraction progresses, allowing the roof to cave behind the shield line forming a mined-out zone known as the gob (or goaf). The cutting device, usually a rotating drum with attached carbide bits known as a shearer, moves up and down the mining face breaking up the coal and knocking it on the conveyor. The face conveyor transports the coal to a larger conveyance system so it can be removed from the mine. The cables that are needed to operate the equipment are attached on the shield side of the conveyor structure or placed in a cable tray (Fig. 1 b). The power center supplies the high-voltage lines needed to power the longwall and is typically located several hundred meters ahead of the face. The power center is periodically advanced as extraction progresses to maintain a safe distance from mining activity.

The longwall extracts a rectangular block of coal known as a panel. Typical panel widths (the mining face dimension) range from 0.2 km to 0.4 km, and panel lengths of 1 km to 4 km are common. The tunnels on either side of the panel are known as gateroads, with the gateroad adjacent to the previously mined panels known as the tailgate and the other known as the headgate. The entries are coated with several centimeters of rockdust, a non-combustible pulverized material, typically limestone, which helps suppress explosions (Fig. 1 c). Often, steel cylinders filled with cement known as "cans" (Fig. 1 d) are used as secondary support to help maintain the integrity of highly stressed gateroads, especially tailgates. A group of adjacent longwall panels separated by gateroads is known as a district. After all the panels are mined, districts are typically sealed with air-tight barriers after which they are no longer accessible or ventilated.

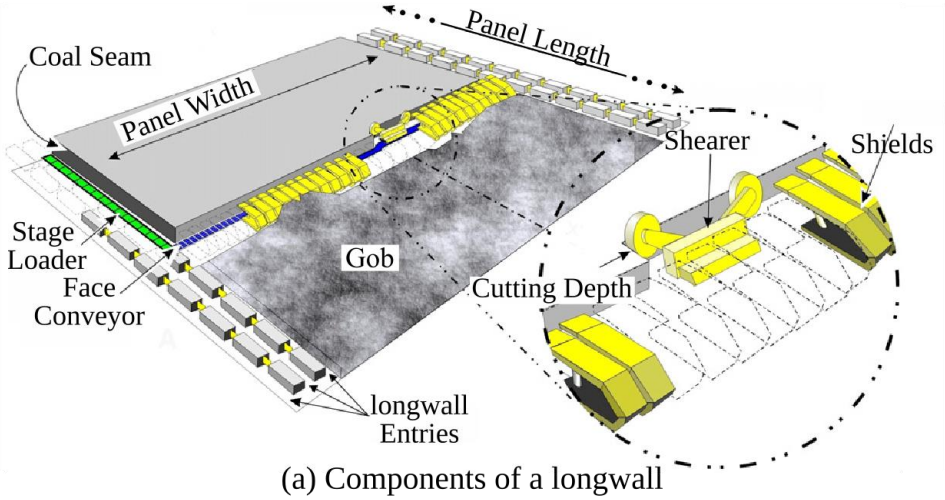


(a) Components of a longwall

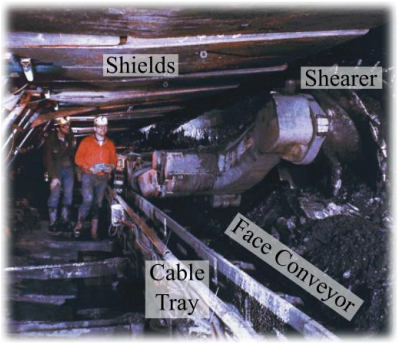


(b) Longwall face


(c) Rockdust application


(d) Support cans

**Fig. 1.** Longwall mining concept. (a) A conceptual diagram of the longwall (modified from [26]), (b) a photograph of a longwall face (modified from [27]), (c) miner applying rockdust in a gateroad (photo in public domain), and (d) installed secondary support cans (modified from [28]).

### *2.2 Distributed Acoustic Sensing*

The DAS IU measures strain, strain rate, or less commonly, deformation rate along the fiber-optic cable. High sampling rates are supported, easily in the kHz range, but data are often decimated to reduce storage demands. Assuming a homogeneous isotropic medium and long seismic wavelengths relative to the interrogator gauge length (L), DAS strain rate measurements ($\dot{\epsilon}$) are equivalent to a finite difference of particle velocities ($\dot{u}$), as would be measured by two fiber-aligned geophones separated by $L$ [29]:

$$\dot{\epsilon}(x,t) = \frac{\dot{u}(x+L/2,t) - \dot{u}(x-L/2,t)}{L} \quad (1)$$

For some DAS interrogators, $L$ (which can be thought of as the length over which strain is averaged) is fixed while others allow setting a custom value at acquisition or in post-processing. Compared to traditional sensors used in mines, DAS offers a much broader frequency response [30], although the exact performance depends on the cable type and coupling, the interrogator and its configuration, and $L$. To avoid signal distortions, the smallest apparent wavelength of the recorded signal of interest should be several multiples of $L$, but smaller values of $L$ also lead to a lower signal-to-noise ratio. This trade-off should be considered in deployment design when using an IU with a fixed gauge length [31].

Another aspect that affects the ability of DAS to monitor seismicity is the phase and orientation dependent sensitivity, which stems from recording strain rather than particle motion typified in conventional geophone sensors [Eq. (1)]. **Fig. 2** shows the amplitude factor for in-plane P and SH plane waves for a horizontal geophone (a) and a DAS fiber with the same alignment (i.e., $0^\circ$), assuming the apparent wavelength is several multiples of $L$ (b). Neither sensor directly records SV waves which are polarized out of plane. The P-wave sensitivities are similar for both sensor types; however, DAS P-wave sensitivity is governed by a $\cos^2(\phi)$ term, whereas the geophone response is governed by $\cos(\phi)$, where $\phi$ is the ray path angle in the X-Y plane measured from the X axis. The S wave sensitivities, however, are significantly different. The DAS response is controlled by a $\frac{1}{2}\sin(2\phi)$ term and the geophone by a $\sin(\phi)$ term. The somewhat surprising result is that DAS is, at least in theory, insensitive to SV plane waves propagating in a direction perpendicular to the fiber, whereas the geophone's maximum sensitivity is in exactly this orientation. Martin et al. [32] provide further details of DAS sensitivities to surfacewave phases, directionality, and gauge lengths.

One of the simplest methods for locating seismicity recorded by linear DAS cables is to assume that the fiber is embedded in a homogeneous, isotropic whole space with a seismic velocity of $v$. When the event is located within the volume defined by the length of the cable, the observed arrival time ($t_A$) for some distance along the fiber ($x$) is related to the event origin time ($t_0$), the shortest distance to the fiber line ($d$), and the fiber distance closest to the event ($x_0$) by the following hyperbolic curve:

$$t_A(x) = \frac{\sqrt{d^2+(x-x_0)^2}}{v} + t_0 \qquad (2)$$

Any of the unknowns in Eq. **(2)** can be solved using phase arrival estimates and common optimization techniques, such as the curve fit implementation in the SciPy library [33]. An important implication of **Eq. (2)** is that the event position in 3D space cannot be determined, only the distance from the fiber and the fiber distance closest to the event can be resolved. This results in a circle of possible event locations around the fiber which all fit the data equally well. However, if multiple linear fiber segments (or other seismic sensors) are available and favorably oriented in relation to a seismic event, absolute locations can be constrained [34].

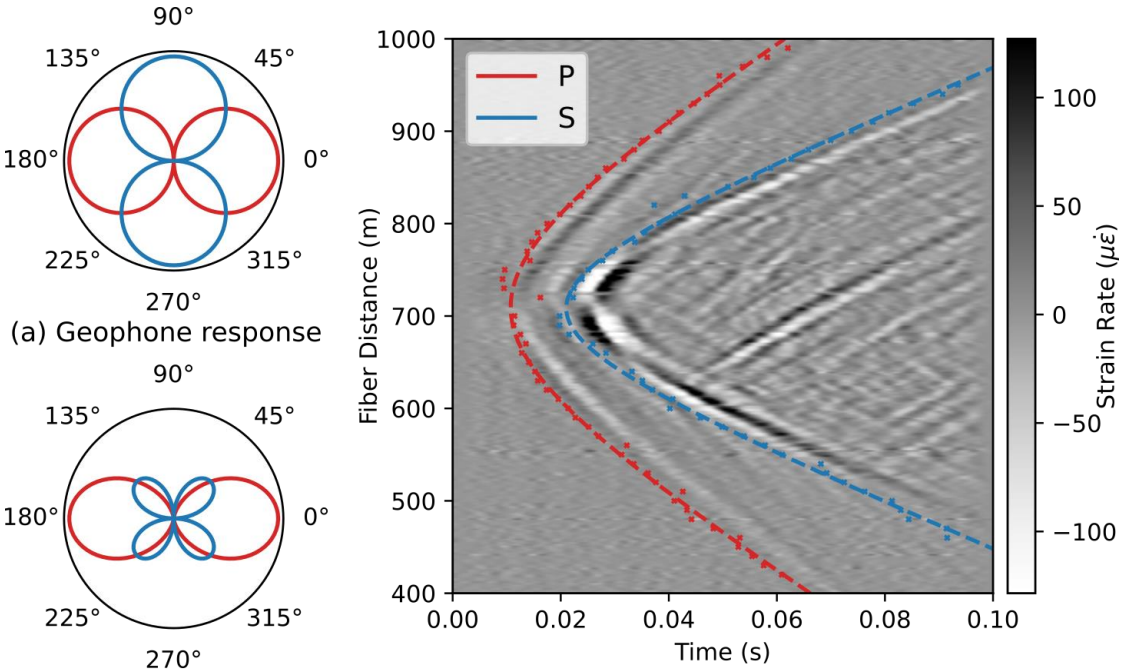


**Fig. 2.** (a) Sensitivity to P (red) and S (blue) waves for a geophone and (b) the sensitivity for a linear DAS fiber oriented along the X axis (0 degrees), assuming apparent wavelengths that are several multiples of the gauge length [35]. (c) An example of fitting Eq. (2) (dotted lines) to manual phase picks (dots) to estimate the location of a seismic event recorded by fiber in a borehole [36].

## 3 Gateroad Deployment

In-mine sensors close to seismic events are valuable for optimizing location accuracy and network sensitivity. Typically, accelerometers or geophones are installed in several shallow boreholes drilled from the mine workings. However, it may be possible to gain similar benefits from the dense recordings of a DAS

cable distributed throughout the mine workings. To test this type of deployment, a fiber-optic cable was installed in a deep US coal mine which has a history of problematic seismicity caused by thick competent strata (TCS) failing in the overburden [37]. The DAS IU was placed in a climate-controlled shelter at the top of a ventilation shaft. Several fiber-optic cables were connected from the shaft, through the mains, and to the active panel with a total fiber length of approximately 7 km. Due to access restrictions, and to be able to monitor both the headgate and tailgate with a single IU, a single cable was placed in the headgate and two fibers in the same cable were spliced together at the end to allow optical signals to travel down and back the entire length of the cable (Fig. 3 a). A 1,280 m section of the cable was placed on the floor and covered with mud (Fig. 1 c), where available, to improve coupling [38], which demonstrably provided a better signal than fiber zip-tied to the roof, ribs, or hung from cable hooks. Unfortunately, a faulty splice connecting the headgate cable to the tailgate cable made the tailgate fiber unusable for recording event waveforms.

During the 47 days of recording, many events with varying magnitudes were visible in the raw (unfiltered) DAS data (Fig. 3 b and c). For the largest magnitude event recorded during the deployment (referred to as event 1, $M = 1.2$), the simple procedure described in **Section 1** applied to P-wave arrivals indicates a distance from the closest point on the cable ($d$), the center channel distance ($x_0$), and velocity ($v$) of $d = 0.45$ km, $x_0 = 0.9$ km, $v = 4.8$ km/s. The estimate of $d$ is close to the horizontal distance of approximately 0.41 km estimated from a catalog created with data from a surface seismic network. The location discrepancy could be rectified if the event occurred some distance into the roof and is acceptable considering that horizontal errors of a few tens of meters are typical for locations derived from surface networks. For a much smaller event occurring on the headgate side of the panel (example event 2, $M = -0.3$) phases are also clearly visible (Fig. 3 c) and the hyperbolic curve fit yields $d = 0.09$ km, $x_0 = 0.63$ km, $v = 4.7$ km/s.

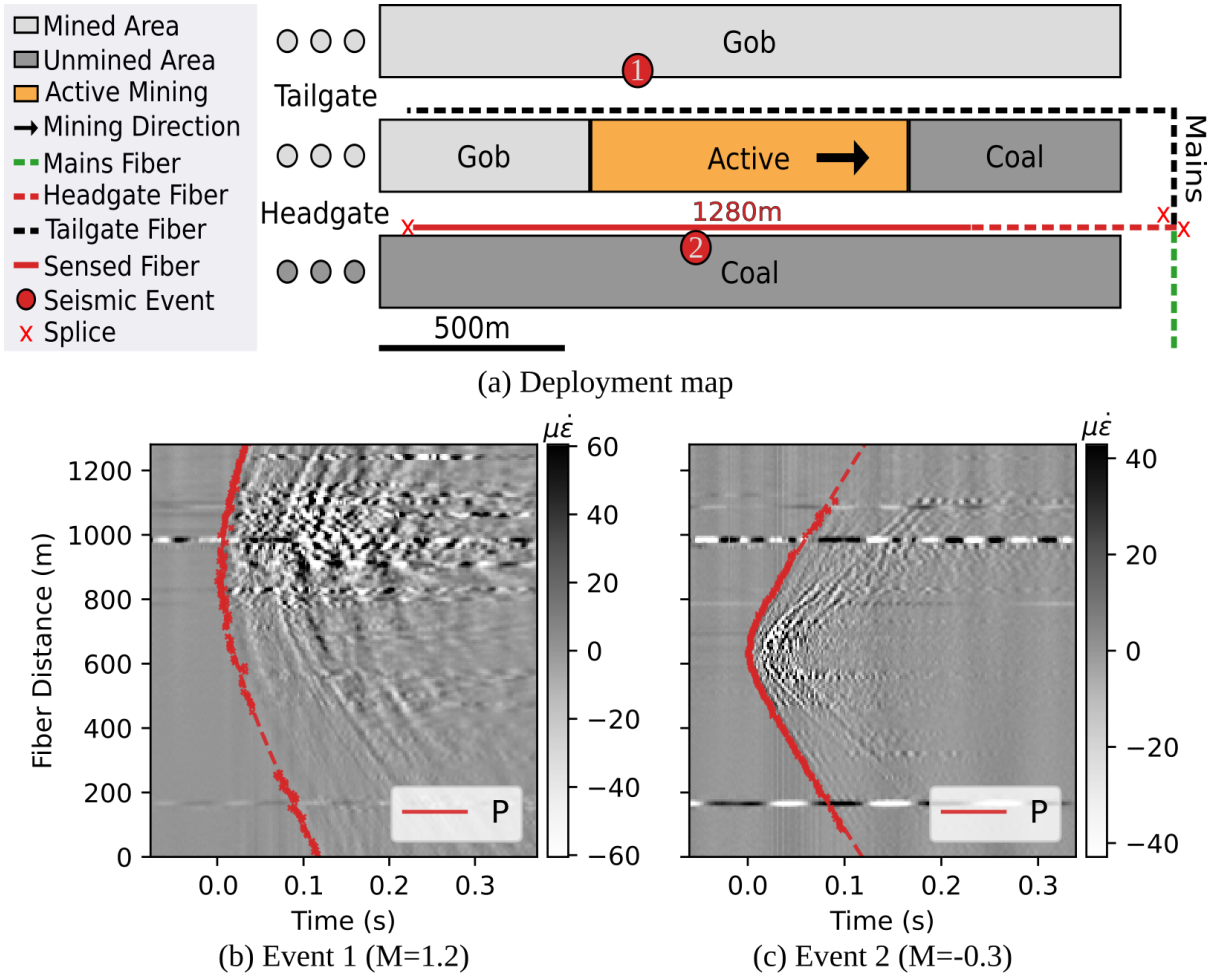


**Fig. 3.** Gateroad deployment and example data. (a) A simplified version of the deployment geometry, truncated panel outlines, the area mined during the deployment, and several other features; (b) The unfiltered strain-rate DAS data for example event 1 located on the tailgate side of the active panel ($M = 1.2$) as well as P-phase picks and a hyperbolic best-fit curve (dashed line); (c) shows the same as (b) but for example event 2 ($M = -0.3$) located on the headgate side of the active panel.

Although the tailgate fiber was not usable for recording event waveforms, a strong reflection at the end of the cable was useful to determine the time and location of cable breaks related to longwall position. Most cable breaks occurred near the active longwall but ranged from nearly 100 m ahead of the face to about 60 m behind it (Fig. 4).

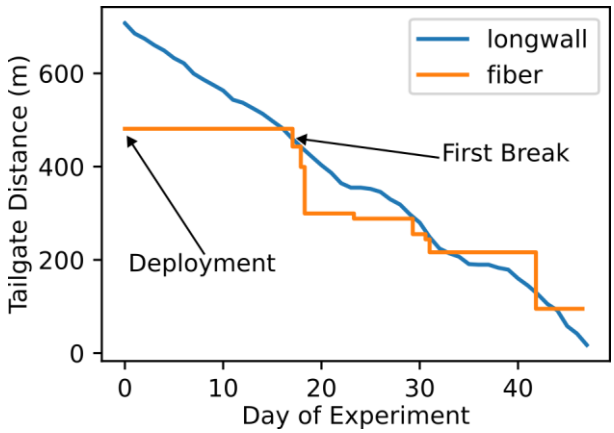


**Fig. 4.** Relative position of the longwall (blue) and tailgate fiber end (orange) with discrete fiber breaks represented by vertical segments in the orange line.

There are several challenges associated with gateroad deployments, namely the need for multiple splices which can compromise the fiber, the susceptibility of the cable to caving or operations-related damage, and potentially lower sensitivity due to less-than-ideal coupling and the rugosity of the damaged excavation surface on which the cable rests. Although du Toit et al. [22] found that fiber tied to mesh was of limited use for recording small ($M < 0$) seismic events in a hardrock mine, Fig. 3 demonstrates that fiber deployed on the mine floor and covered with mud is useful for detecting and locating both larger events ($M > 1$) several hundred meters from the fiber and smaller events ($M < 0$) originating closer to the fiber.

While some progress has been made on this dataset, additional work is needed to develop and refine pre-processing workflows to improve signal-to-noise ratios of body wave phases. Additionally, determining best practices to optimize cable survival will be important before mines can routinely and robustly use this deployment strategy. Moreover, if durable fiber can be distributed throughout the mine gateroads, it could not only match or exceed the event detection and location capabilities of traditional in-mine microseismic systems, but may also be useful for other DFOS-related safety applications such as detecting thermal events in mined-out areas [39]. However, due to limitations discussed later, utilizing some conventional sensors, either in the mine or on the surface, in conjunction with this deployment strategy is prudent.

## 4 Surface Borehole Deployment

When seismic sensors are installed from mine workings in a single seam, or exclusively on the surface, accurately estimating the depths of seismic events is challenging because the sensor geometry is nearly planar. To address this limitation, seismic sensors can be positioned both near the seam and on the surface and/or in a borehole [40]. DAS shows promise to densely probe the seismic wavefield in horizontally stratified layers typically found in coal mines. This section presents two examples of DAS deployments which help constrain the vertical coordinates of seismic events in the vicinity of underground coal exploitation.

The first example shows a fiber-optic cable grouted in a vertical borehole drilled from the surface over a gateroad of an active panel. The DAS data and geophones installed in the same borehole were used to locate induced seismicity. Fig. 5 (a) shows an event recorded by this configuration. In this case, a more sophisticated location scheme than the one presented in **Section 2.2** was employed. The DAS strain-rate data were transformed into a probability grid using matched field processing techniques [41]. The grid served as a prior in the location algorithm, which incorporated P- and S-wave first arrivals from the geophones to better vertically constrain the event depth (Fig. 5 b). After applying this workflow, all the located events shift above the seam from their original locations determined with only geophone data. Using only a sparse geophone array leads to a mirroring effect, i.e., locations above and below the seam fit the data equally well. This effect, in addition to the reduction in other sources of errors provided by using a greater number of sensors, accounts for the large shift (up to 200 m) between the two sets of locations. The locations that combine DAS and geophone data (Fig. 5 purple dots) is superior to the locations determined with geophones only (Fig. 5 gray dots).

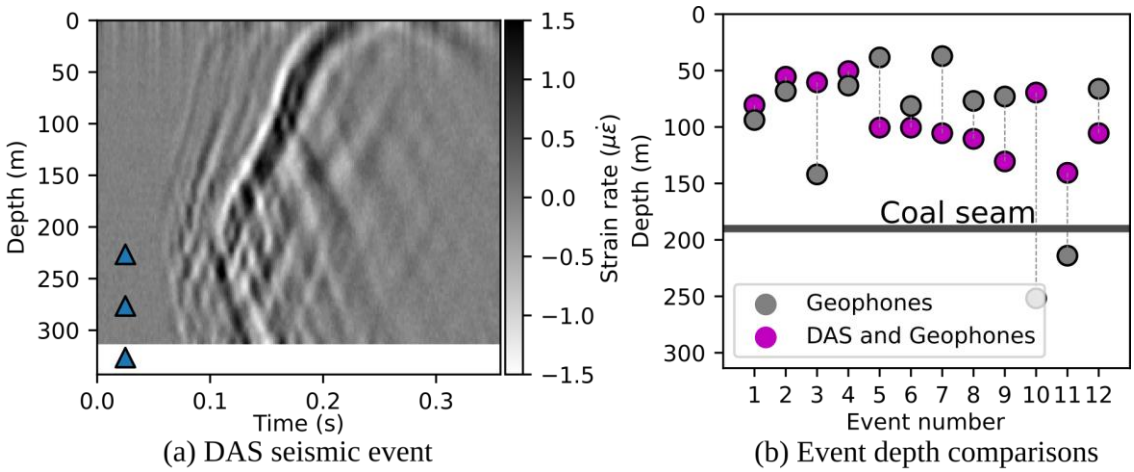


**Fig. 5.** Vertical borehole DAS data. (a) An example event recorded on a fiber in a vertical borehole. The blue triangles indicate the depths of the tri-axial geophones in the borehole with the fiber. (b) Event locations using only geophone data and including DAS data.

In the second example, a fiber-optic cable was grouted into a directional borehole drilled from the surface and curved horizontally under the coal seam. Over 100 nodes (portable, self-contained geophone stations [13]) were deployed on the surface (Fig. 6 a). The goals of the experiment were to explore the utility of the DAS data in locating and understanding seismicity, and to assess and calibrate an event location procedure using the node data. To that end, a small calibration blast was detonated from the coal seam which was recorded clearly in the DAS data (Fig. 6 b).

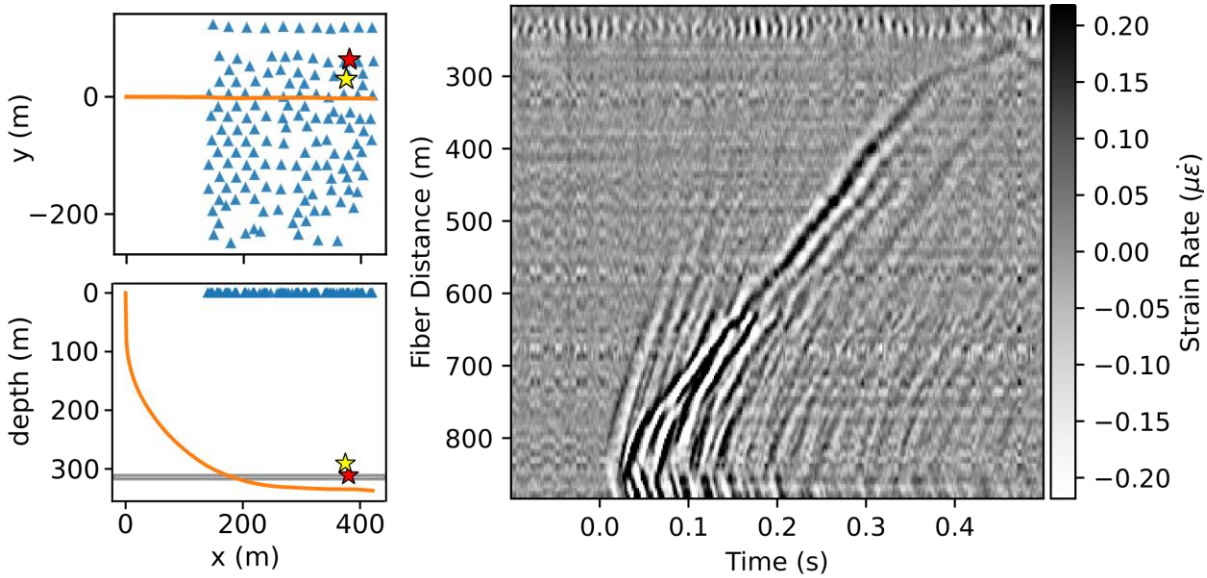


(a) Deployment map and profile (b) DAS shot record

**Fig. 6.** Directional borehole DAS data. (a) Deployment map (top) and profile view (bottom) where the blue triangles are the surface nodes, the red star indicates the true location of a calibration blast, the yellow star indicates the calculated location of the calibration blast, the orange line is the fiber, and the gray horizontal bar indicates the location of the coal seam. (b) DAS recording of a calibration blast.

These two examples demonstrate that DAS deployments in surface boreholes can provide a clear picture of event-induced strain fields which can help improve event location estimates, particularly in depth. The borehole cable also has the advantage of being isolated from mine operations, which reduces noise contamination and risk of damage associated with operating equipment. However, in both cases, extraction-induced ground motions were severe, and the cable was sheared several times as the longwall advanced. Fig. 7 shows the position of the longwall as various breaks occurred in the DAS cable. Other disadvantages of this deployment type include the requirements of a borehole and infrastructure for protecting, powering, and communicating with the DAS IU. Of course, these disadvantages are mitigated if suitably located boreholes already exist (e.g., exploration or degassing holes) and surface infrastructure or fiber lines to other structures are readily available. Moreover, vertical wells instrumented with DAS fiber are useful in vertical seismic profiling (VSP) [42], which could be used to build a velocity model for other surface-based seismic deployments or to monitor time-dependent changes in the near-fiber geological structure.

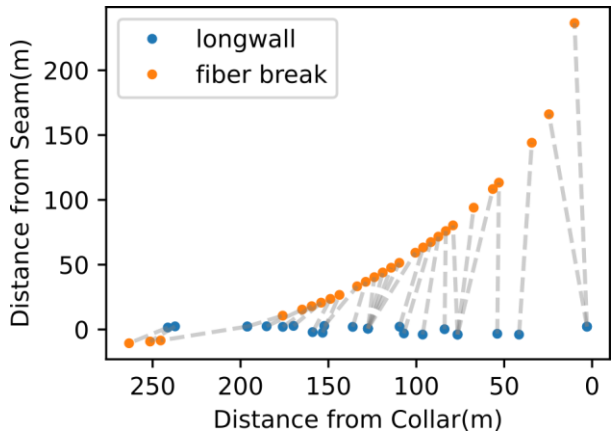


**Fig. 7.** Horizontal and vertical position of the longwall and associated fiber breaks in the directional borehole. All but 2 of the 28 breaks occurred between 30m behind and 30m ahead of the longwall.

## 5 In-mine Borehole Deployment

DAS can also be deployed in boreholes drilled from the mine level. One objective of such a deployment is to monitor the mechanical behavior of undermined massive strata which can cause myriad ground control issues if proper caving is not achieved [43]. In this experiment a DAS cable was installed in a near-horizontal borehole drilled from mine level into a thick competent sandstone (Fig. 8 a and b). The mine experienced coal bursts on the mining face (i.e., face bursts) with contributing factors being thickness and strength of the near-seam TCS, high-strength brittle coal, and significant depth of cover (0.65 km). The DAS IU was located at the longwall's power center several hundred meters from the mining face. The cable included three fiber coupling configurations, illustrated in Fig. 9 which are: fiber suspended from the roof by cable hooks, fiber zip-tied to metal mesh on the roof, and fiber inserted into the borehole. The fiber was inserted by taping it to threaded sections of polyvinyl chloride (PVC) rods and manually pushing the rods into the hole. Unlike the deployments detailed in **Section 4**, the fiber was not grouted in the borehole which certainly resulted in lower fidelity measurements of rock strain.

The experiment lasted for about 10 days as the longwall advanced from approximately 20 m behind the borehole to 20 m ahead of it. During the deployment, a regional seismic network located 50 events near the mining area which ranged in magnitude from 1.1 to 2.2 (Fig. 8 c). A temporary increase in the background noise level of the borehole fiber was observed when the shearer was operating and a permanent increase (on

297 day 9) as the cable sustained damaged due to large deformations in the TCS. These phenomena are easily
298 observed by averaging the root mean square (RMS) strain rate of all borehole channels for two-minute
299 increments (Fig. 8 c). Locations and times of breaks in the fiber, and presumably the surrounding rock, were
300 identified by first low-pass filtering, decimating, and concatenating many hours of DAS data. The filter-
301 induced Gibbs effects at the end of the cable define the farthest point of optical transmission (Fig. 8 d).
302 Interestingly, both the borehole and zip-tied fiber acquired high-amplitude signals with identifiable apices
303 for events occurring on the headgate side of the panel (Fig. 8 e).

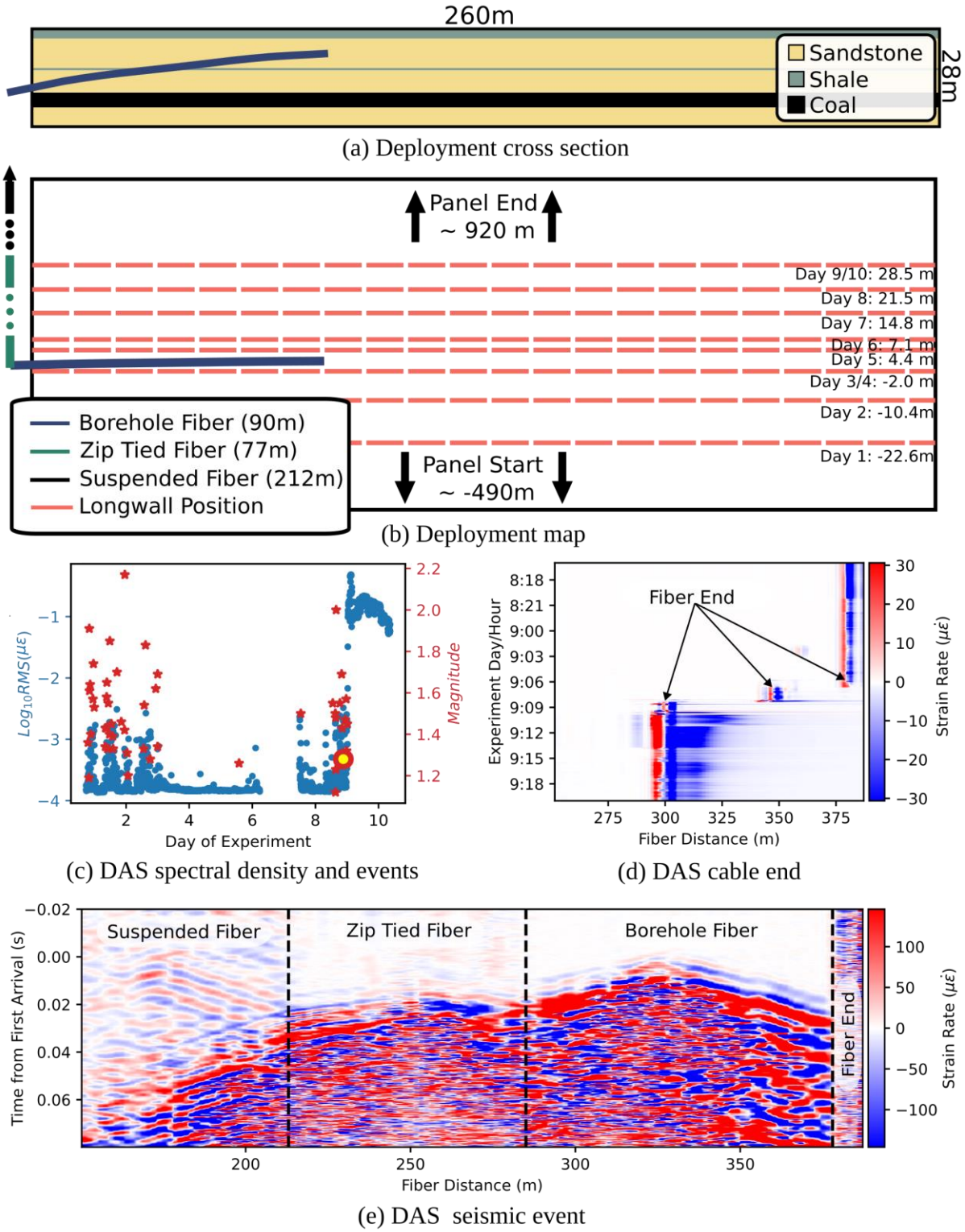


**Fig. 8.** In-mine near-horizontal borehole fiber deployment. (a) Cross section of the near-seam geology and the location of the sensing fiber (blue line). (b) Map view of the deployment with three types of fiber and longwall positions as a function of experiment duration. (c) Seismic events detected by a regional network (red) as well as the logarithm of the average root mean square strain rate for every two minutes of DAS data (blue).

(d) Changes in the end of the cable which broke in two segments over the course of a few hours on day 9. (e) Example data of a *M* 1.3 event, the red dot with yellow center in (c), on the three types of fiber.

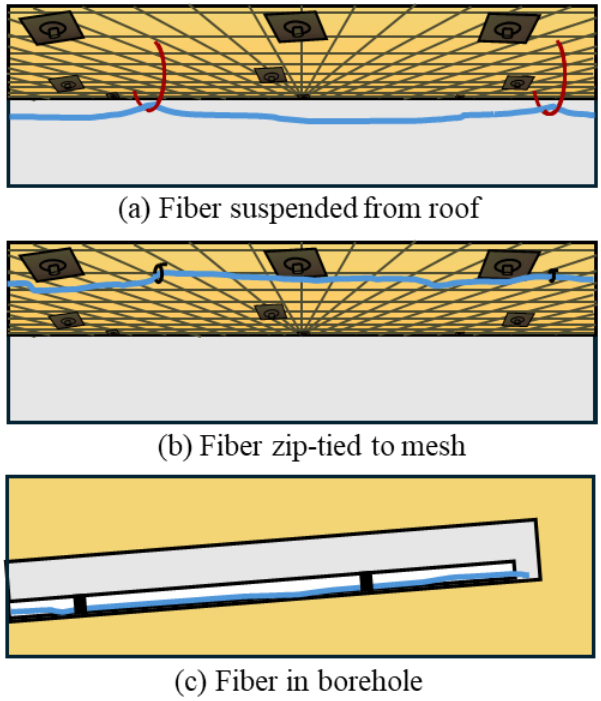


**Fig. 9** Different coupling methods used for the fiber cable in the in-mine borehole deployment. (a) Fiber (blue) suspended by the roof from cable hooks, (b) fiber zip-tied to the mesh, and (c) fiber in the un-grouted borehole taped to the PVC insertion rod.

This type of deployment could provide several types of useful geomechanical information. First, the mechanisms of coal bursts are not well understood and vary from mine to mine. For example, some of the proposed face bursts' mechanisms involve a sudden failure of TCS above the gob which then causes a rapid redistribution of stress on the face, while others propose that the primary failure occurs entirely in or near the coal seam without any significant dynamic contribution of the TCS [44,45]. Direct measurements in the TCS as these failures occur could shed additional light on these physical processes, which, in turn, could enable more informed, site-specific, coal burst mitigation strategies. Second, it may be possible to characterize damage progression by identifying and tracking acoustic emissions occurring near the fiber, perhaps similar to the laboratory procedure outlined by Zafar et al. [46]. Third, interferometric techniques [47] may be able to identify time-dependent seismic velocity or attenuation changes indicative of progressive TCS failure near the fiber.

The main disadvantage of this type of deployment is the need to drill a horizontal borehole from seam level, which can be labor intensive and costly. The sub-optimal coupling of the fiber in our case could also be an issue as grouting the fiber in place would provide better rock strain signals. However, leaving the cable ungrouted also allows it to slip as the TCS undergoes large strains and thereby enabling the collection of more data before the fiber fails.

## 6 Longwall Face Deployments

Another intriguing possibility for DAS is to monitor areas of the mine that would be largely impractical to deploy traditional sensors, such as on the longwall face itself. This would be particularly useful when face bursting is a known hazard. This section details two experiments in the same mine mentioned in **Section 5** which experienced face bursts (Fig. 10 a). Chambers and Shragge [24] describe the first deployment which used a new kind of seismoacoustic array (Fig. 10 b) composed of two fiber configurations: "lead cables"' and "microphones." The lead cables were standard tight-buffered signal cable fastened to the hydraulic hoses connecting the longwall shields. The second configuration consisted of fiber-optic microphones which were thin-walled plastic cylinders wrapped with 90 m of tight-buffered fiber, resulting in a solid yellow appearance. The IU measured changes in circumferential strain in the cylinder due to fluctuations in air pressure, thus allowing sounds in the audible range to be recorded. For the second deployment, a cable was simply inserted into the cable tray (Fig. 1 b). In both deployments the DAS IU was co-located with the longwall's power station about 400 m from the face on the headgate side of the panel.

The lead cables of the seismoacoustic array recorded the vibrations excited by the face bursts' elastic wavefield, and the microphones recorded the burst-related sound waves propagating in the workings. Examples of both types of waveforms recorded by the array for a $M = 1.8$ face burst, as well as the first-arrival picks and the best fit hyperbolic curve, are shown in Fig. 10 c, using Eq. **(2)** and the optimization scheme already described, $d = 0$ m, $x_0 = 130$ m, $v = 1.9$ km/s. Considering about 30 face bursts over several shifts, the lead cable waveforms tended to be impulsive, meaning estimating phase arrival times is feasible and are useful for identifying the event apex which coincides with $d$. The microphone channels are more emergent and could be used for quantifying damage location and severity. For example, Fig. 10 d

shows the binned apex location for the events, as well as the microphone root mean square (RMS) strain rate, a proxy for acoustic energy, as a function of face distance. The maximum microphone RMS occurs between the center of the panel and the tailgate, which, anecdotally, coincides with the most severe face bursts for this panel. The events with apices on the edge of the array might not have occurred on the mining face.

Unfortunately, the data from the cable tray deployment were less useful. Although the events were clearly visible, as well as the location of the shearer before the event (Fig. 10 e), the background noise levels were too high to make accurate arrival time picks even after applying a variety of common filtering techniques. The event coda location and duration, however, likely coincide with the settling of ejected coal and therefore might be used as a proxy for burst damage. Moreover, with more advanced filtering and noise suppression, the signals may become usable.

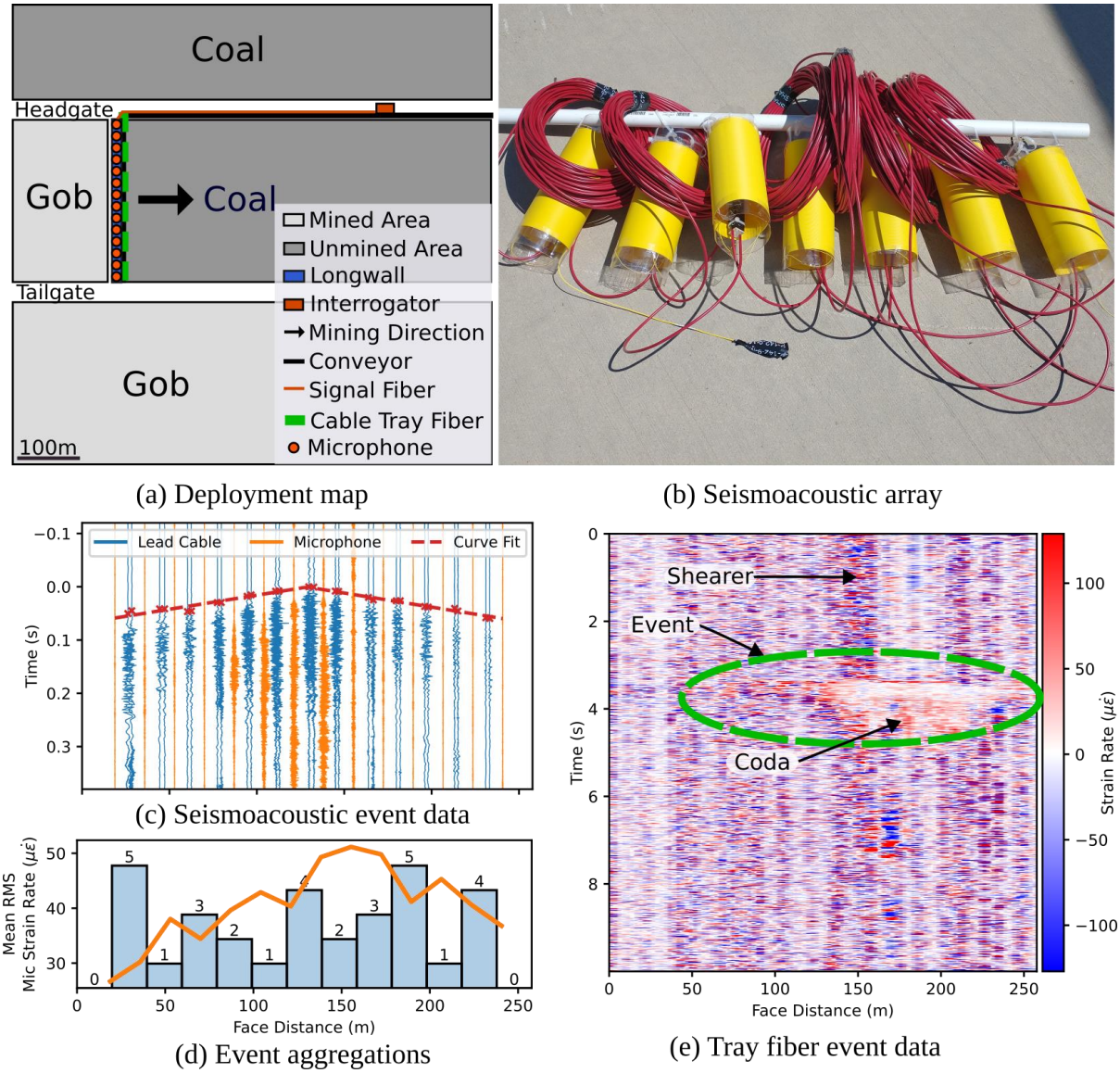


**Fig. 10.** Longwall face deployments. (a) Deployment geometry map. (b) Part of the seismoacoustic array consisting of lead cables (red) and microphones (yellow). (c) Waveforms from the lead cable (blue) and microphone (orange) from a $M = 1.8$ face burst. The first-arrival picks (red Xs) and the best-fit hyperbolic curve (dashed red line) are also shown. (d) The binned apex locations determined from the lead cable channels (blue bars) and the average microphone RMS acoustic strain rate (orange line) for 1.0 s of data after the first arrival for the 30 face bursts recorded by the seismoacoustic array. (e) Example data from the cable tray deployment recording a different $M = 1.8$ face burst.

The deployments detailed in this section could be useful in addressing face burst risks by providing quantitative data on face burst location and severity (acoustic power or coda duration). These measures in

turn could guide tactical and strategic efforts to mitigate related risks. They also have the huge advantage of rarely needing reconfiguration; the sensors move with the mining face and the IU could be relocated at the same time as the substation, requiring very little routine maintenance provided the cables on the longwall remain intact.

These longwall-centered deployment strategies on their own, however, would be much less useful for monitoring other types of seismicity, such as events occurring in overburden strata or gateroad pillars. Also, because the array is located so close to the mining equipment, it will be much less sensitive than fiber deployed in quieter sections of the mine. Since the cable is not directly coupled to the rock, and there will be complex geometries and equipment interactions, it would be extremely difficult to ascertain anything beyond arrival times from these data. Moreover, the uncertain coupling and shifting geometry make identifying which seismic phases the array records challenging, and since the array is so close to the source, near field phases are likely [48].

## 7 Support Can Deployment

As mentioned in **Section 2.1**, cement-filled steel cans (Fig. 1 d) are commonly used for secondary support. As the cans take weight from the roof and floor converging, micro-cracks associated with the excavation damage are forced closed and unconsolidated materials under and above the cans are compacted. This allows for efficient transmission of elastic waves through the cans, which could be measured by wrapping them with fiber. This type of deployment might complement deploying cable on the mine floor or ribs which can experience significant free-surface amplifications and "ringing" due to poor rock coupling. Unlike cable deployed on the floor, the can dilation is sensitive to vertical strain, providing an additional direction of strain-field sampling. Moreover, as quasi-static loading progresses, the circumference of the cans increases due to Poisson's effect. Measuring the long-term changes in circumferential strain may be useful for understanding stress redistribution. Low-frequency DAS processing, which has been used for several years in the oil and gas industry [49] and for monitoring enhanced geothermal systems [50], may be able to provide such measurements.

To test these theories, six different support cans were tightly wrapped with approximately 20 m of fiber in the headgate of an active longwall mine (Fig. 11 a). The cans were spaced 3 m apart, had a height of 3 m, and a diameter of 0.6 m. Between the cans, cable was deployed on the gateroad floor in the same fashion mentioned in **Section 3**. Composite strain rate time series were created for each can by first removing a nearly constant strain rate mean of 1.1 με̇ from all channels, then averaging the center 12 m of strain recordings of each can. Data from fiber that might be close to the end of the wrap were not used to avoid including any cable that might be sensitive to non-can strain. For larger events ($M > 1$), the unfiltered floor strain rate channels had 1 to 6 times higher signal-to-noise ratios (SNR), and 5 to 20 times higher amplitudes compared to the can signals recorded in the same vicinity (Fig. 11 b). The can signals, however, tend to have more impulsive first arrivals.

To estimate change in can circumferential strain over the duration of the experiment, a 5-second moving window average was applied to every second of can strain-rate data. The moving average operator acts as a low-pass filtering, smoothing, and decimation operation and is more efficient than applying these steps sequentially. The strain-rate data were then integrated along the time axis to yield an estimate of change in circumferential strain for the approximately 40-hour experiment duration (Fig. 11 c). The two cans subjected to a front abutment load during much of the experiment (cans 1 and 2) experienced an overall dilation, whereas cans 3 and 4 experienced an increase before decreasing to less than their initial values. Can 5 exhibited a near constant decrease to a final strain of about -0.3% and can 6 experienced a significant increase before returning to nearly the same level as at the start of the experiment.

It is odd that cans 3, 4, and 6 would experience an increase, then decrease considering they were located behind the longwall for the entire recording period. Under idealized conditions, the abutment load in these areas would decrease as mining progresses. However, in this mine the overburden is dominated by competent sandstones and there are certainly complex caving behaviors occurring which could transfer stress, particularly from adjacent mined-out panels, in atypical ways. The drastic decrease in strain observed in can 5 could be explained by the fiber slackening and slipping rather than reflecting deformation of the can surface. Certainly, more experience with this type of deployment is needed to determine how robustly DAS is able to measure can strain, and validation with common instruments such as borehole pressure cells inserted into the coal or pressure plates placed between the can and roof would be a prudent next step. A

Brillouin-based distributed strain sensing (DSS) system could also interrogate a different fiber in the same cable to get a more direct static strain measurement.

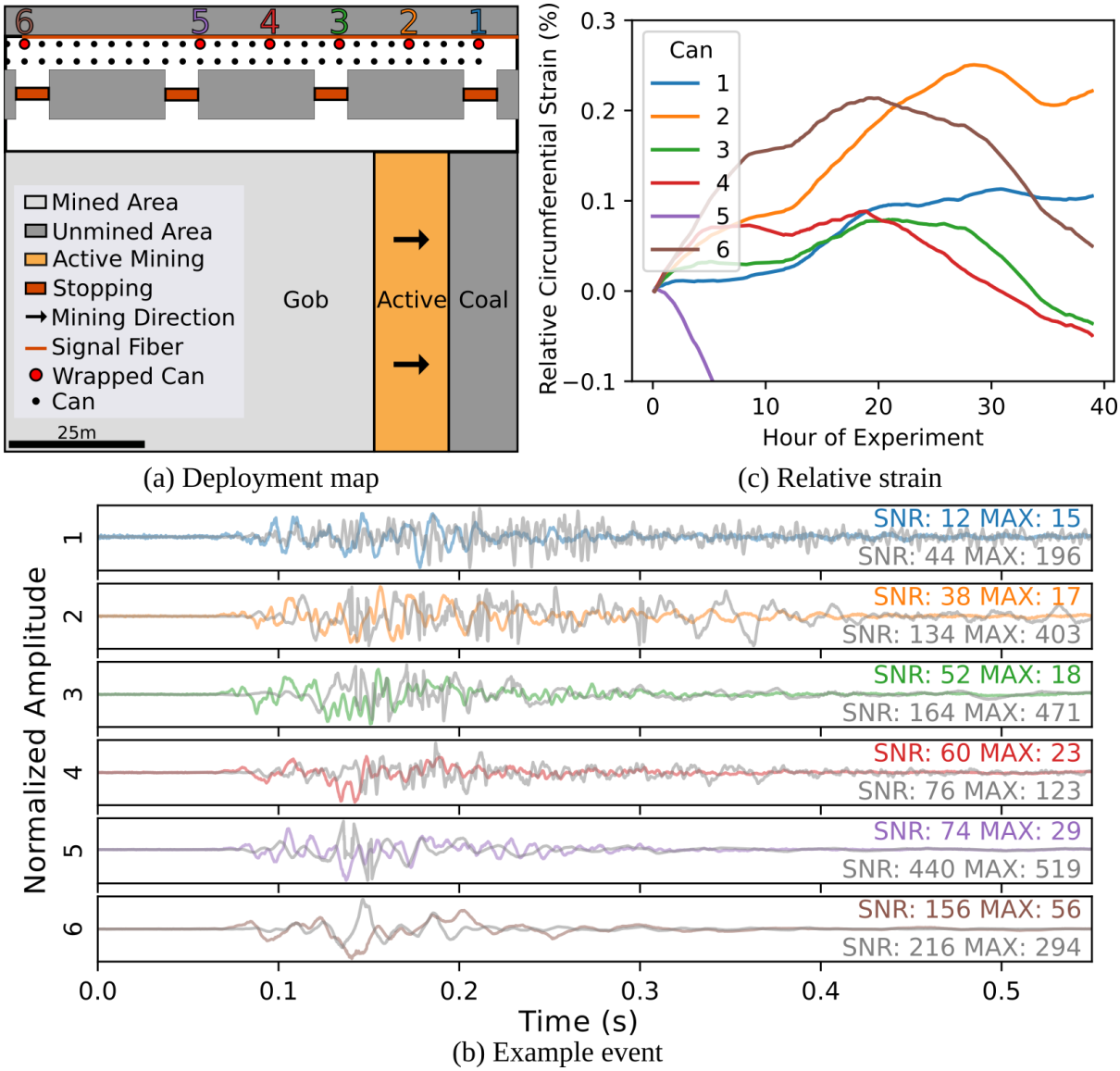


**Fig. 11.** Can deployment. (a) Deployment map showing wrapped cans (labeled 1-6). The DAS IU is located several hundred meters to the right of the mining face. (b) Example event ($M = 1.5$) recorded by the can loops (colored) and nearest fiber deployed on the mine floor (gray) where each signal has been detrended and normalized to its maximum value. The signal-to-noise ratios (SNR) and maximum signal amplitudes (MAX) are listed in each plot. (c) Low-frequency can strain from DAS data. Can 5 decreases nearly monotonically to a minimum strain of approximately -0.003; however, the whole plot is not shown as to avoid obscuring detail of the other cans.

# 8 Discussion

Table 1 displays summary information about each deployment type including examples of objectives it can meet, the monitoring domain (part of the mine), common causes of fiber-optic cable failure, and some miscellaneous notes. The following sections discuss strengths, challenges, practical lessons, and avenues of future research.

Table 1 Summary of DAS Deployment Types.

| | Gateroad | Surface Borehole | In-Mine Borehole | Longwall Face | Support Can |
|---|---|---|---|---|---|
| **Objectives** | Improve event location, sensitivity, and focal mechanism resolvability | Improve event location, sensitivity, and focal mechanism resolvability | Study strata caving behaviour | Monitor seismicity and damage on the mining face | Track changes in abutment stress; sample vertical strain field |
| **Domain** | Panel or district | District | Section of a panel | Mining face | Panel |
| **Cause of Cable Failure** | Floor heave, rockfalls, equipment interaction | Strata shear displacement (often in front of the longwall) | Strata caving | Equipment interaction, ejected rock | Rockfalls, excessive support can deformation |
| **Notes** | Careful planning of cable placement and splicing is prudent | Requires grouting the cable | Generally for short-term (days to weeks) monitoring | Very high noise; only practical for large events | The quality of the support can wrapping affects measurement quality |

## *8.1 Additional DAS Advantages for Longwall Coal Mines*

In addition to long sensing length, potential to deploy fiber in return air, and near-source recordings, a few other benefits of DAS to longwall mines are worth mentioning. First, most mines already have extensive experience with fiber-optic installations for communications, much of which is transferable to DFOS applications. In a practical sense, this means mine personnel could deploy fiber, repair fiber breaks, and connect sensing segments into existing infrastructure without much additional training. All measurements of a single IU are naturally time-synchronized whereas synchronizing conventional seismic equipment, especially when located underground, is much more challenging.

Because spatially dense DAS recordings contain more wavefield information than sparse point sensors, they have some significant advantages. First, it is much easier to identify seismic phases based on their apparent velocity which makes arrival time estimation easier and reduces the risk of mislabeling phases. Second, more signal processing routines are available for dense spatially sampled data, such as F-K filtering, which can remove signals with non-seismic propagation speeds. Finally, the wave propagation information in the DAS records could alleviate the need for frequent calibration blasts as velocity estimations can be made from the recorded data (e.g., Fig. 2 c, Fig. 3 b and c, Fig. 6 b).

### *8.2 Challenges and Opportunities*

DAS has some disadvantages and barriers to adoption in coal mines. First, because it is a relatively new approach to passive seismic monitoring, several data processing areas are not yet mature. These include dealing with variable ground coupling quality and estimating source parameters such as event magnitude, energy, and moment tensors from DAS data. A pragmatic approach to overcome these challenges is the use of hybrid networks. Arrival time and polarity information from dense DAS data can improve event locations, quantify propagation effects, and help constrain focal mechanism inversions. Data from conventional, in-mine, or surface networks can then be used to estimate source parameters. Second, DAS IUs are still relatively expensive, typically ranging from 100,000 USD to 250,000 USD. Unless a mine routinely experiences damaging seismic events, this level of investment may be difficult to justify. Third, most mine sites are unprepared, in terms of experience and computation infrastructure, to handle the large volumes of data a DAS IU can produce, which can reach several Terabytes per day. The use of emerging machine learning tools [51] and specialized open-source software [52] for analysis of DAS data may help overcome these challenges. Finally, there are multiple reasons DAS data can become unusable, including poor coupling, faulty splices, high background noise levels, and breaks in the cable. These issues can be mitigated with improvements to deployment design. In fact, all of the strategies outlined in this paper will require such improvements to increase the chances of long-term survival in the rugged mining environment.

### *8.3 Practical Deployment Lessons*

Several important lessons were learned from the field deployments. First, apart from the cable being damaged by mining equipment, splices are the most likely failure point in a fiber array and therefore should always be appropriately protected such as in a splice tray or outdoor-rated splice protector. Second, an optical time domain reflectometer (OTDR) trace is much better for assessing splice quality than the estimate provided by a fusion splicer. Third, one can mitigate data loss risk by designing the optical path such that the segments of fiber most likely to sustain damage are as close to the end of the path as possible. Fourth, when connecting a sensing cable to a mine's fiber-optic infrastructure, even "obviously true" assumptions about the fiber system should be verified. For example, during the experiment in **Section 3** several hours were wasted tracking down a previously undocumented splice which connected fibers of different colors between the top of the ventilation shaft and the bottom. Lastly, correct interrogator configuration can make the difference between recording high-quality signals versus instrument noise. Consulting with the DAS manufacturer and bringing reference configuration documentation to the field are prudent measures.

### *8.4 Future Work*

In the opinion of the authors, there are several important research steps needed to accelerate routine DAS monitoring in longwall coal mines. First and foremost, is to continue to conduct DAS coal mine deployments and improve data processing methodologies. Perhaps the first step in this direction is to move beyond processing paradigms which either require an overly simplified velocity model (as was used here) or neglect to take advantage of the strong spatial relationships inherent in DAS data by treating each DAS channel as an independent measurement. The spatial relationships between channels can help in filtering, arrival time estimation, phase association, etc.

More field research on cable survival and sensitivity is needed. Building on previous work to relate cable configuration to signal quality in underground mines [21], long-term deployments of various cable types in different configurations (e.g., trenched, laying on the surface, in tight conduit) which are nearly collocated would provide valuable information that might lead to general recommendations and standard deployment practices. For example, the static strain distribution on each configuration will provide insight into cable failure locations and modes, and the recording of common events can be used to make sensitivity comparisons.

## 9 Conclusions

Because DAS poses no explosion risks and can collect spatially dense recordings over many kilometers, it is well suited for use in underground coal mines. This study details several DAS deployment strategies that have potential to improve geotechnical monitoring in longwall coal mines. These strategies can meet a variety of objectives including: augmenting conventional networks to improve routine monitoring of seismicity, quantifying damage from coal bursts occurring on the mining face, observing geomechanical behavior of undermined strata, and monitoring static and dynamic stress on secondary support systems. Although these nascent fiber-optic sensing applications will require additional research and development to improve both data processing and deployment robustness before they can be used routinely in underground mines, the underground coal mining industry stands to gain significant safety benefits from DAS technology.

## 10 Acknowledgements

We would like to thank various mining operations for allowing us to conduct DAS research in their mines and for providing other forms of support. We would also like to thank Terra15 for answering our questions and providing technical support for many of these experiments. We would also like to thank the following people who helped in planning or implementing at least one of the deployments: Jim Garner, Will Ray, Matthew Tascione, Frantisek Stanek, Dhari Alharbi, Sean Bemis, Amna Alashkhari, Karen Williams, Erik Westman, Martin Chapman, and Gabriel Walton. We also thank Virginia Tech Advanced Research Computing for resources. This research was supported in part through the NSF IUCRC Center to Advance the Science of Exploration to Reclamation in Mining. The findings and conclusions in this report are those of the author(s) and do not necessarily represent the official position of the National Institute for Occupational Safety and Health, Centers for Disease Control and Prevention or any other employer of the listed authors. Mention of any company or product does not constitute endorsement by NIOSH, CDC. The authors declare they are free of competing interests.

## 11 References

[1] Durrheim RJ. Mitigating the risk of rockbursts in the deep hard rock mines of South Africa: 100 years of research. Extracting the Science: A Century of Mining Research, Brune J (Eds), Society for Mining, Metallurgy, and Exploration, Inc 2010:156–71.

[2] Simser BP. Rockburst management in Canadian hard rock mines. Journal of Rock Mechanics and Geotechnical Engineering 2019;11:1036–43.

[3] Potvin Y. Strategies and tactics to control seismic risks in mines. Journal of the Southern African Institute of Mining and Metallurgy 2009;109:177–86.

[4] Mendecki AJ, Lynch RA, Malovichko DA. Routine micro-seismic monitoring in mines. Australian Earthquake Engineering Society 2010 Conference, 2010, p. 1–33.

[5] Hudyma M, Potvin YH. An Engineering Approach to Seismic Risk Management in Hardrock Mines. Rock Mech Rock Eng 2010;43:891–906.

[6] Meyer S, Lynch R. Microseismic monitoring and short term hazard assessments in underground coal mines. Recent Advances in Rock Engineering (RARE 2016), Atlantis Press; 2016, p. 446–9.

[7] Cheng G, Tang C, Li L, Chuai X, Yang T, Wei L. Micro-fracture Precursors of Water Flow Channels Induced by Coal Mining: A Case Study. Mine Water Environ 2021;40:398–414.

[8] Luxbacher K, Westman E, Swanson P, Karfakis M. Three-dimensional time-lapse velocity tomography of an underground longwall panel. Int J Rock Mech Min Sci 2008;45:478–85.

[9] Cao W, Durucan S, Cai W, Shi J-Q, Korre A. A physics-based probabilistic forecasting methodology for hazardous microseismicity associated with longwall coal mining. Int J Coal Geol 2020;232:103627.

[10] Leśniak A, Śledź E, Mirek K. Detailed Recognition of Seismogenic Structures Activated during Underground Coal Mining: A Case Study from Bobrek Mine, Poland. Energies 2020;13:4622.

[11] Swanson P, Boltz MS, Chambers D. Seismic Monitoring Strategies for Deep Longwall Coal Mines. National Institute for Occupational Safety and Health; 2016.

[12] Boltz MS, Chambers DJ, Hanson DR. Evaluating Seismicity at Underground Coal Mines Using Temporary Surface Geophone Deployments. 52nd US Rock Mechanics/Geomechanics Symposium, American Rock Mechanics Association; 2018.

[13] Dean T, McGuiness J, Bona A. Microseismic monitoring of an underground longwall mine using a modern lightweight nodal recording system. Fourth International Meeting for Applied Geoscience & Energy, Society of Exploration Geophysicists and American Association of Petroleum Geologists; 2024, p. 198–202.

[14] Swanson P, Stewart C, Koontz W. Installation of a digital, wireless, strong-motion network for monitoring seismic activity in a western Colorado coal mining region. Symposium on the Application of Geophysics to Engineering and Environmental Problems 2007, Society of Exploration Geophysicists; 2007, p. 559–65.

[15] Hartog AH. An introduction to distributed optical fibre sensors. CRC press; 2017.

[16] Webster P, Wall J, Perkins C, Molenaar M. Micro-Seismic Detection using Distributed Acoustic Sensing. Seg Technical Program Expanded Abstracts 2013. https://doi.org/10.1190/SEGAM2013-0182.1.

[17] Lindsey NJ, Martin ER, Dreger DS, Freifeld B, Cole S, James SR, et al. Fiber-optic network observations of earthquake wavefields. Geophys Res Lett 2017;44:11–792.

[18] Spica ZJ, Perton M, Martin ER, Beroza GC, Biondi B. Urban Seismic Site Characterization by Fiber-Optic Seismology. J Geophys Res [Solid Earth] 2020;125:1251.

[19] Lindsey NJ, Martin ER. Fiber-optic seismology. Annual Review of Earth and Planetary 2021;49:303–36.

[20] Cunningham E, Lord N, Fratta D, Chavarria A, Thurber C, Wang H. Three-dimensional distributed acoustic sensing at the Sanford Underground Research Facility. Geophysics 2023;88:WC209–20.

[21] Zeng X, Wang HF, Lord N, Fratta D, Coleman T. Field Trial of Distributed Acoustic Sensing in an Active Room-and-Pillar Mine. In: Yingping Li, Martin Karrenbach, Jonathan B. Ajo-Franklin, editor. Distributed Acoustic Sensing in Geophysics: Methods and Applications, Wiley; 2021, p. 65–79.

[22] du Toit HJ, Goldswain G, Olivier G. Can DAS be used to monitor mining induced seismicity? Int J Rock Mech Min Sci 2022;155:105127.

[23] Luo X, Duan Y. A field trial of distributed optic fiber sensing technique for longwall caving mapping. Rockburst and Seismicity in Mines, Society for Mining Metallurgy and Exploration; 2022.

[24] Chambers D, Shragge J. Seismoacoustic Monitoring of a Longwall Face Using Distributed Acoustic Sensing. Bull Seismol Soc Am 2023;113:1652–63.

[25] Peng SS. Longwall Mining, 3rd Edition. CRC Press; 2019.

[26] Karacan C. Modeling and prediction of ventilation methane emissions of U.S. longwall mines using supervised artificial neural networks. Int J Coal Geol 2008;73:371–87.

[27] Einicke G, Ralston J, Hargrave C, Reid D, Hainsworth D. The Application of Smoothing within Longwall Mine Navigation. Proceedings of the International Global Navigation Satellite Systems Society IGNSS Symposium, 2009, p. 1–3.

[28] Mark C. Coal bursts in the deep longwall mines of the United States. International Journal of Coal Science & Technology 2016;3:1–9.

[29] Wang HF, Zeng X, Miller DE, Fratta D, Feigl KL, Thurber CH, et al. Ground motion response to an ML 4.3 earthquake using co-located distributed acoustic sensing and seismometer arrays. Geophys J Int 2018;213:2020–36.

[30] Lindsey NJ, Rademacher H, Ajo-Franklin JB. On the broadband instrument response of fiber-optic DAS arrays. J Geophys Res [Solid Earth] 2020;125. https://doi.org/10.1029/2019jb018145.

[31] Dean T, Cuny T, Hartog AH. The effect of gauge length on axially incident P-waves measured using fibre optic distributed vibration sensing. Geophys Prospect 2017;65:184–93.

[32] Martin ER, Lindsey NJ, Ajo-Franklin JB, Biondi BL. Introduction to Interferometry of Fiber-Optic Strain Measurements. In: Yingping Li, Martin Karrenbach, Jonathan B. Ajo-Franklin, editor. Distributed Acoustic Sensing in Geophysics: Methods and Applications, Wiley Online Library; 2021, p. 111–29.

[33] Virtanen P, Gommers R, Oliphant TE, Haberland M, Reddy T, Cournapeau D, et al. SciPy 1.0: fundamental algorithms for scientific computing in Python. Nat Methods 2020. https://doi.org/10.1038/s41592-019-0686-2.

[34] Verdon JP, Horne SA, Clarke A, Stork AL, Baird AF, Kendall J-M. Microseismic monitoring using a fiber-optic distributed acoustic sensor array. Geophysics 2020;85:KS89–99.

[35] Benioff H. A linear strain seismograph. Bull Seismol Soc Am 1935;25:283–309.

[36] Staněk F, Jin G, Simmons J. Fracture Imaging Using DAS-Recorded Microseismic Events. Front Earth Sci Chin 2022;10. https://doi.org/10.3389/feart.2022.907749.

[37] Van Dyke MA, Su WH, Wickline J. Evaluation of seismic potential in a longwall mine with massive sandstone roof under deep overburden. Int J Min Sci Technol 2018;28:115–9.

[38] Harmon N, Rychert CA, Davis J, Brambilla G, Buffet W, Chichester B, et al. Surface deployment of DAS systems: Coupling strategies and comparisons to geophone data. Near Surf Geophys 2022;20:465–77.

[39] Liu TY, Meng XJ, Wang FQ, Li RC, Hou MY, Wang ZW, et al. Fibre optic sensor for coal mine combustion detection. Mining Goes Digital, London: CRC Press; 2019, p. 647–52.

[40] Lynch R. Microseismic Monitoring of Underground Coal Mines: Objectives, Warnings and Sensor Array Design. Proceedings of the 18th Coal Operators' Conference, ro.uow.edu.au; 2018, p. 31–8.

[41] Gal M, Reading AM, Rawlinson N, Schulte-Pelkum V. Matched field processing of three-component seismic array data applied to Rayleigh and love microseisms. J Geophys Res [Solid Earth] 2018;123:6871–89.

[42] Correa J, Egorov A, Tertyshnikov K, Bona A, Pevzner R, Dean T, et al. Analysis of signal to noise and directivity characteristics of DAS VSP at near and far offsets — A CO2CRC Otway Project data example. Lead Edge 2017;36:994a1–7.

[43] Gray I, Gibbons T. Longwall behaviour in massive strata. Proceedings of the 2020 Coal Operators' Conference, University of Wollongong; 2020, p. 47–13.

[44] Iannacchione AT, Tadolini SC. Occurrence, predication, and control of coal burst events in the U.S. International Journal of Mining Science and Technology 2016;26:39–46.

[45] Rice GS. Bumps in coal mines—theories of causes and suggested means of prevention or of minimizing effects. Transactions of the American Institute of Mining and Metallurgical Engineers 1936;36:3–23.

[46] Zafar S, Hedayat A, Moradian O. Evaluation of Crack Initiation and Damage in Intact Barre Granite Rocks Using Acoustic Emission. Geo-Congress 2020 2020:399–408.

[47] Yang J, Shragge J. Long-term ambient seismic interferometry for constraining seasonal subsurface velocity variations in urban settings: a distributed acoustic sensing (DAS) case study. Geophys J Int 2023;234:1973–84.

[48] Luo B, Jin G, Stanek F. Near-field strain in distributed acoustic sensing-based microseismic observation. Geophysics 2021;86:49–60.

[49] Jin G, Roy B. Hydraulic-fracture geometry characterization using low-frequency DAS signal. Lead Edge 2017;36:975–80.

[50] Titov A, Dadi S, Galban G, Norbeck J, Almasoodi M, Pelton K, et al. Optimization of enhanced geothermal system operations using distributed fiber optic sensing and offset pressure monitoring. Proceedings of the SPE hydraulic fracturing technology conference and exhibition, 2024. https://doi.org/10.2118/217810-MS.

[51] Tourei A, Martin ER, Ankamah AT, Hole JA, Chambers DJA. An autoencoder-based deep learning model for enhancing noise characterization and microseismic event detection in underground longwall coal mines using distributed acoustic sensing monitoring. 58th US Rock Mechanics/Geomechanics Symposium 2024. https://doi.org/10.56952/arma-2024-0207.

[52] Chambers D, Jin G, Tourei A, Issah AHS, Lellouch A, Martin E, et al. DASCore: A Python library for distributed fiber optic sensing. Seismica 2024;3. https://doi.org/10.26443/seismica.v3i2.1184.

## 12 Appendix A: DAS IU Configuration

Table 2 DAS IU configuration for each experiment. Abbreviations used: PW is pulse width, GL is gauge length, FL is fiber length, dt is time sampling interval, and dx is spatial sampling interval (also called channel spacing)

| Experiment | Manufacturer | Model | Pulse Width (m) | Gauge Length (m) | Fiber Length (km) | dt (ms) | dx (m) |
|---|---|---|---|---|---|---|---|
| Gateroad (Section 3) | Terra15 | Treble | 5.7 | 5.7 | 7.1 | 0.5 | 5.7 |
| Vertical Surface Borehole (Section 4) | Terra15 | Treble | 7.4 | 7.4 | 1.5 | 0.35 | 2.5 |
| Directional Surface Borehole (Section 4) | Terra15 | Treble + | 9.8 | 9.8 | 1.4 | 0.15 | 4.9 |
| In-mine Borehole (Section 5) | Terra15 | Treble | 4.1 | 8.1 | 0.5 | 0.13 | 1.6 |
| Seismoacoustic (Section 6) | Terra15 | Treble | 10.6 | 21.2 | 3.0 | 0.12 | 5.7 |
| Cable Tray (Section 6) | Terra15 | Treble | 5.7 | 11.4 | 1.3 | 0.2 | 2.5 |
| Support Can (Section 7) | Terra15 | Treble | 5.7 | 11.4 | 0.8 | 0.17 | 2.45 |